Electronic Supplementary Material (ESI) for Journal of Materials Chemistry C.

Supporting Information

Y_2(Ge,Si)O_5:Pr Phosphors: Multimodal Temperature and Pressure Sensors Shaped by Bandgap Management

Małgorzata Sójka[1], Marcin Runowski[2,*], Przemysław Woźny[2], Luis D. Carlos[3], Eugeniusz Zych[1,*], Stefan Lis[2]

[1] University of Wroclaw, Faculty of Chemistry, 14. F. Joliot-Curie Street, 50-383 Wroclaw, Poland

[2] Adam Mickiewicz University, Faculty of Chemistry, Uniwersytetu Poznańskiego 8, 61-614 Poznań, Poland

[3]Phantom-g, CICECO-Aveiro Institute of Materials, Physics Department, University of Aveiro, 3810-193 Aveiro, Portugal

1. Vacuum referred binding electron diagrams of $Y_2(Ge_x,Si_{1-x})O_5$ host lattices

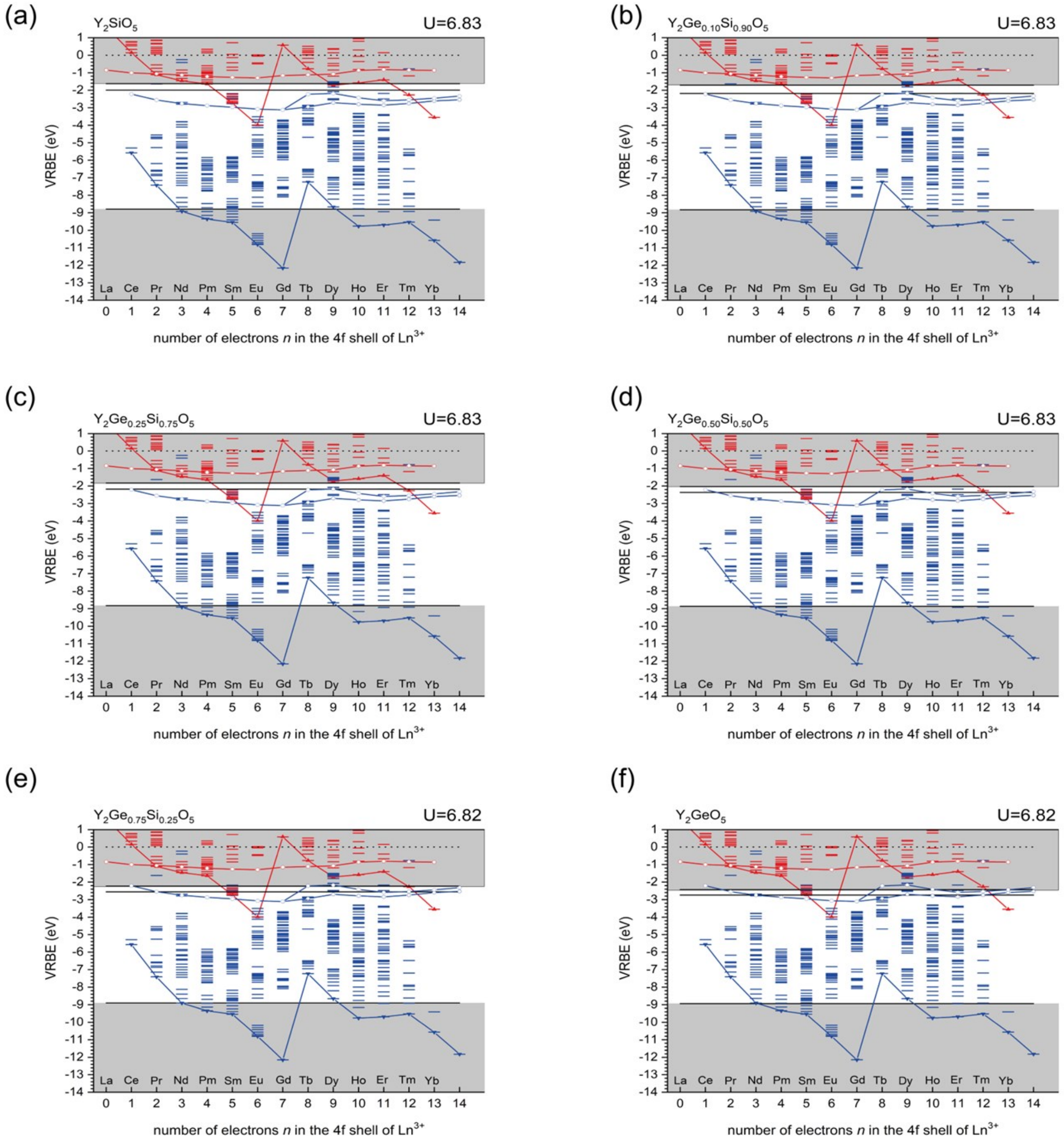

Figure S1. VRBE diagrams of $Y_2(Ge_x,Si_{1-x})O_5$ solid solutions. The data for the diagrams were taken from papers published by Dorenbos[1–3] who developed this very useful methodology to relate the host bands and activator's electronic levels to each other. A proper values which were used to construct VRBE diagrams are presented in Table S1.

2. Structural properties

Figure S2a,b presents details of the local symmetry of the two different Y^{3+} sites (marked as Y1 and Y2) in the isostructural Y_2SiO_5 and Y_2GeO_5 compounds. In both structures the trivalent yttrium ions are located in two non-equivalent sites, both with *C1* symmetry but different coordination numbers (CN) of 7 (Y1) and 6 (Y2).[4] It is expected that the Pr^{3+} ion, having a larger ionic radius than Y^{3+} (1.27 A, 0.96 A, respectively[5] for CN = 7), occupies mostly the larger Y1 site, for which CN and, consequently, the RE-O distances are larger. This postulate comes from the results of EPR studies of LSO:Ce and YSO:Ce monocrystals, in which far more of the Ce^{3+} ions, similarly large as Pr^{3+}, are located in Y1 sites.[6,7]

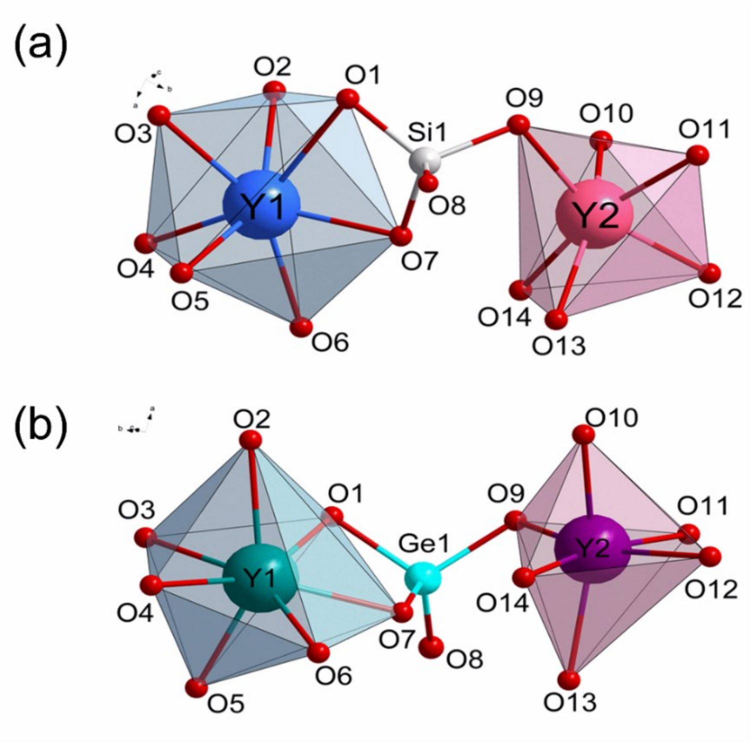

Figure S2. The coordination spheres of Y^{3+} ions in the two different sites offered by (a) Y_2SiO_5, (b) Y_2GeO_5.[8,9]

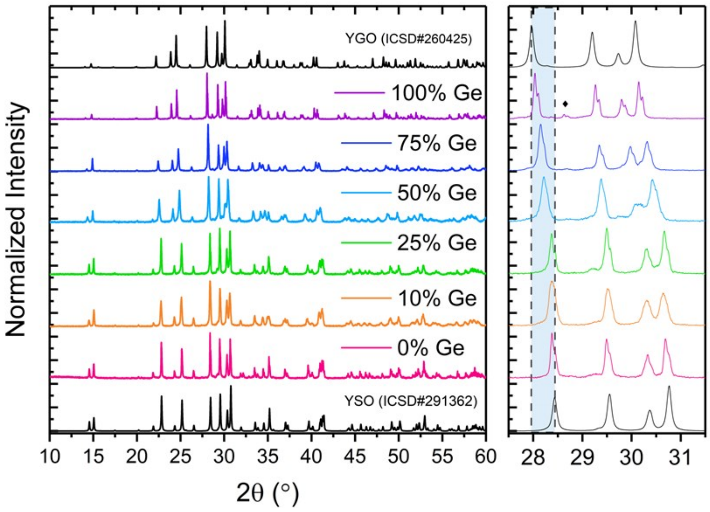

Figure S3. The recorded XRD patterns of the investigated $Y_2(Ge_x,Si_{1-x})O_5$:Pr phosphors. The black dotted lines emphasize the shift of the diffraction lines towards lower angles with the increasing Ge content.

3. **Photoluminescent properties**

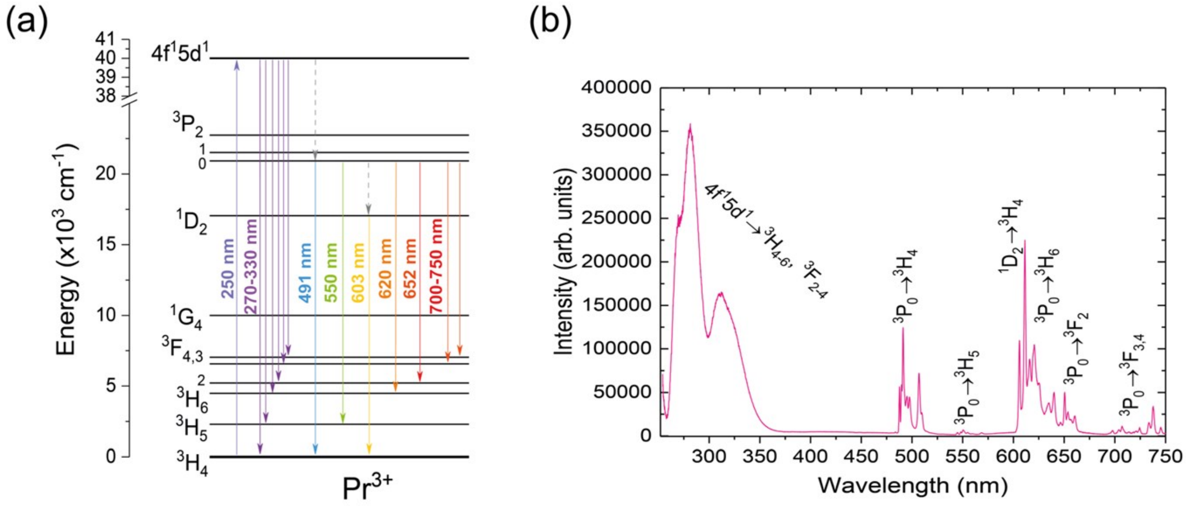

Figure S4. (a) Scheme of the energy level diagram of Pr^{3+} with indicated emission transitions and their characteristic wavelengths. (b) emission spectrum of the $Y_2(Ge_{0.25},Si_{0.75})O_5$:Pr recorded at 11 K under 250 nm excitation. Assignment of the emission features to the transitions of the Pr^{3+} ion is also given in (b).

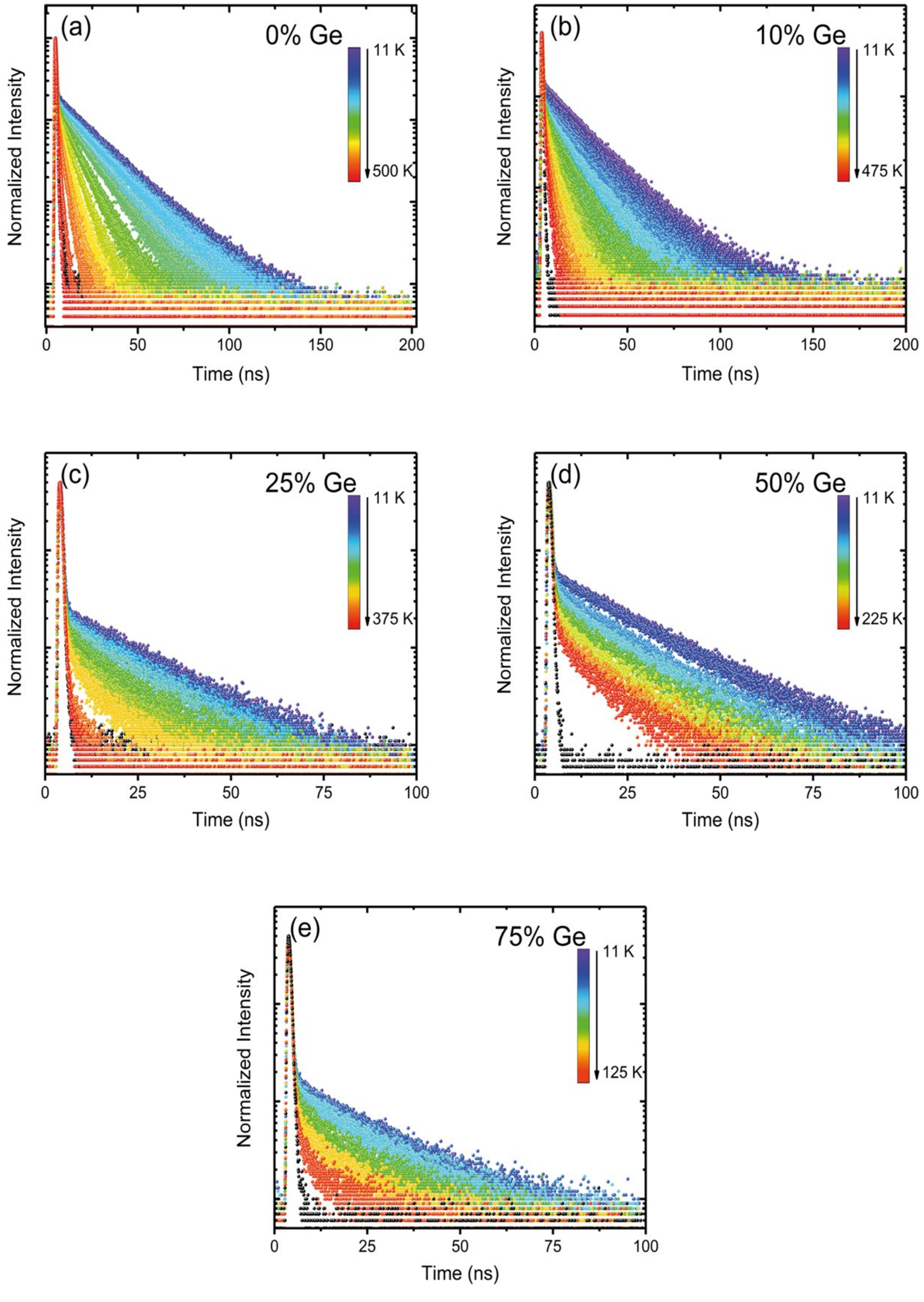

Figure S5. Decay traces of the 5d→4f luminescence of the $Y_2Ge_x,Si_{1-x}O_5$:Pr phosphors under 250 nm excitation where (a) x = 0 %, (b) x = 10%, (c) x = 25%, (d) x = 50%, (e) x = 75%**.** Instrumental response function (IRF) is also given (black dots) in each panel.

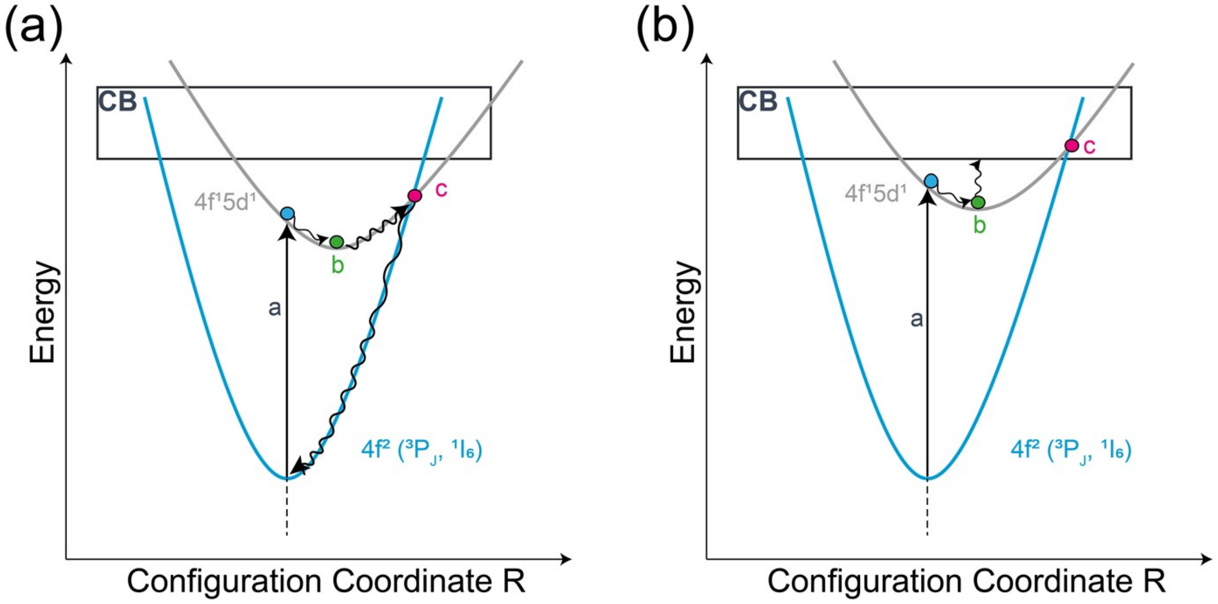

Figure S6. Schematic configuration coordinate diagram presenting quenching mechanism of the 5d→4f luminescence through (a) cross-over process, (b) thermally activated photoionization.

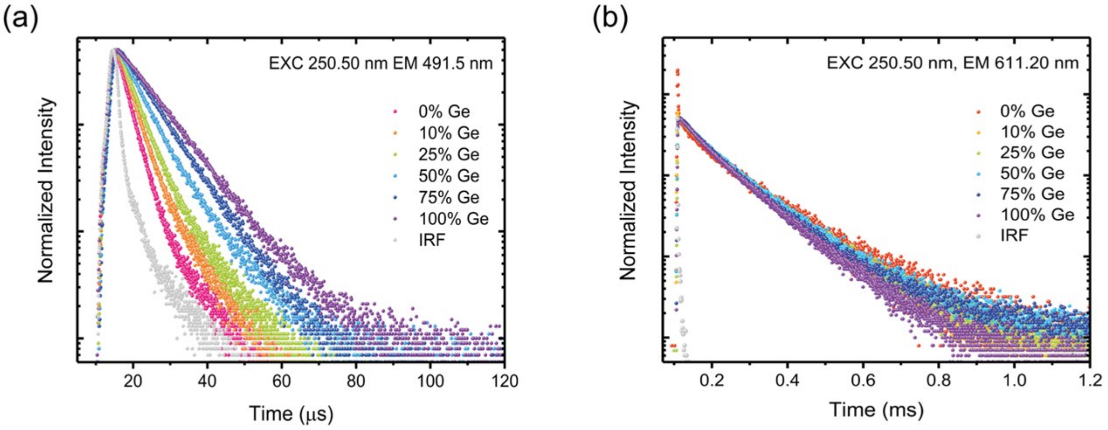

Figure S7. Decay traces of the (a) $^3P_0$ and (b) $^1D_2$ luminescence of the $Y_2(Ge_x,Si_{1-x})O_5$:0.05%Pr phosphors recorded at RT under 250.50 nm excitation. The corresponding calculated decay times are presented in Table S3.

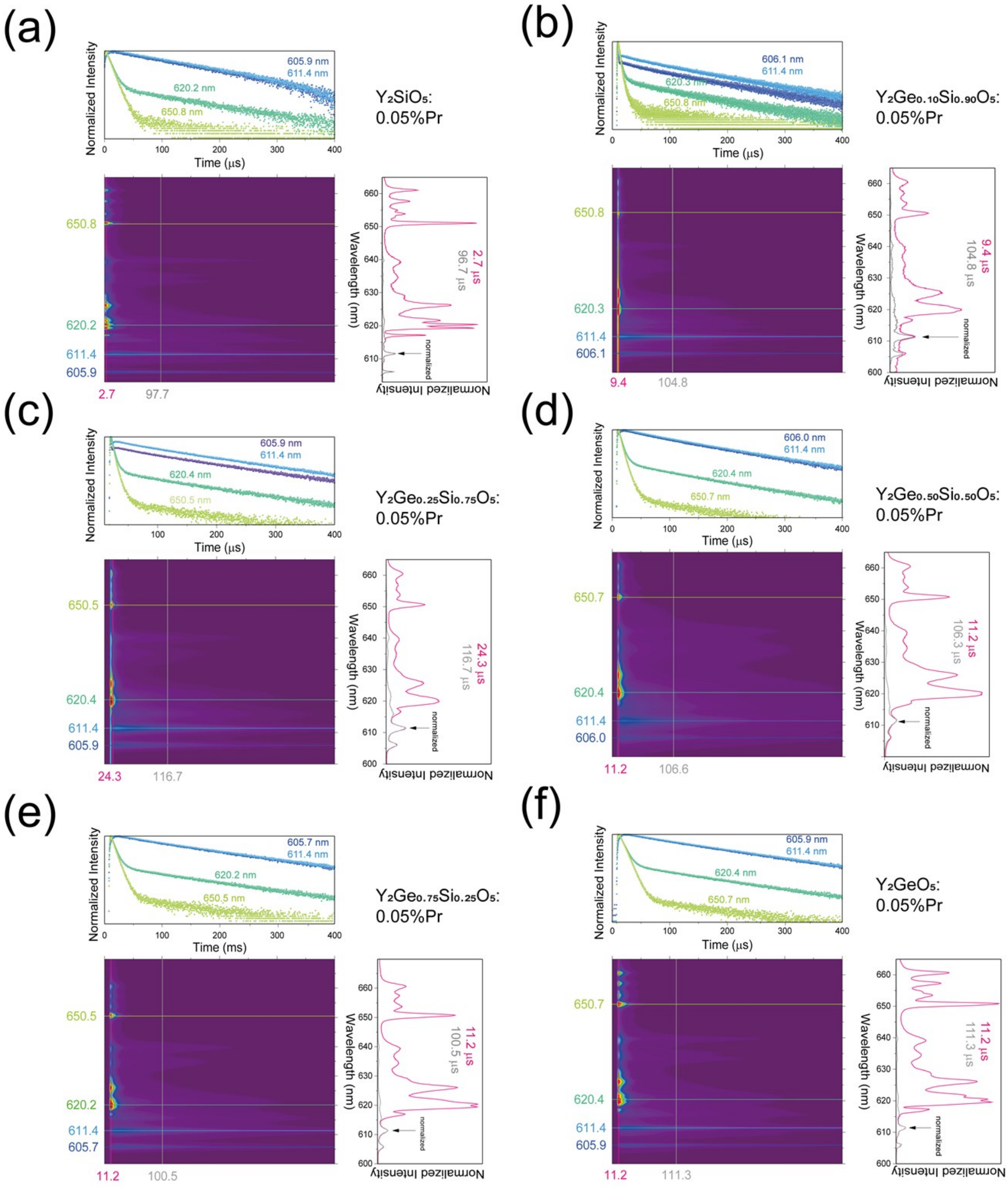

Figure S8. Time-resolved luminescence measurements upon excitation at 250 nm recorded at 11 K for each of the investigated materials.

4. **Thermometric properties**

For the calculations of thermometric parameters based on intensity (*I*) of emission bands, the spectra were converted from photon flux per constant wavelength interval function into photon flux per energy (*E*) interval by means of Jacobian transformation[10,11], see Eq. S1:

$$f(E) = f(\lambda)\frac{d\lambda}{dE} = f(\lambda)\frac{d}{dE}\left(\frac{hc}{E}\right) = - f(\lambda)\frac{hc}{E^2}, \qquad (S1)$$

where h represents Planck constant and c is the speed of light in a vacuum. The minus in the equation can be ignored as it only points to different integration directions in E and λ.

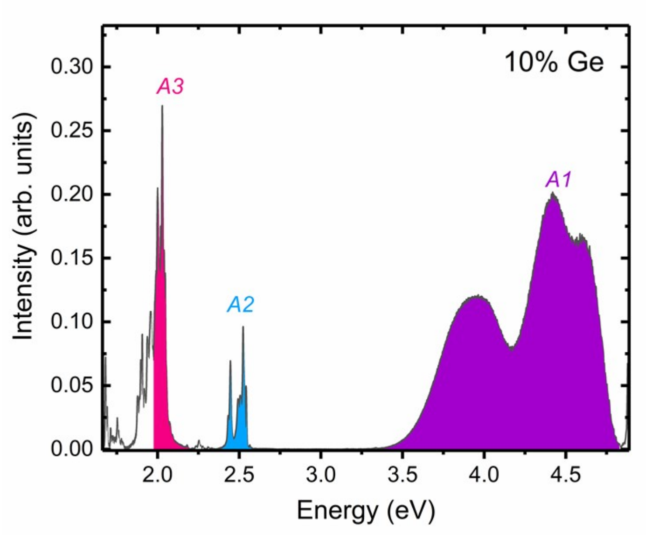

Figure S9. Representation of areas of spectra (A1, A2, A3) which were used in thermometric analysis. An analogous approach was used for all investigated compositions.

The integrated areas (I_i) of the 5d→4f and 4f→4f luminescence were calculated using Eq. S2:

$$I_i = \int_{E_1}^{E_2} \Gamma(E,T)\, dE, \qquad (S2)$$

The relative uncertainty of the integrated areas, *δI/I*, were estimated with Eq. S3:

$$\left(\frac{\delta I}{I}\right)^2 = \int_{E_1}^{E_2} \left[\left(\frac{\delta\Gamma}{\Gamma}\right)^2 + \left(\frac{\delta E}{\Delta E_s}\right)^2\right] dE, \qquad (S3)$$

where δE represents uncertainty in the energy step (ΔE_s) which is given as a product of the detection slit widths (0.20-0.25 mm) and reciprocal of the linear dispersion of the diffraction grating (1.8 nm/mm), $\delta\Gamma/\Gamma$ stands for relative uncertainty on intensity. The latter was calculated by estimation of the signal-to-noise ratio (*SNR*) in each analysed spectrum(*δI/I*). This parameter was calculated by dividing the readout fluctuations of the baseline (calculated as the standard deviation of a given spectral region) by the maximum intensity value of the transition under integration.

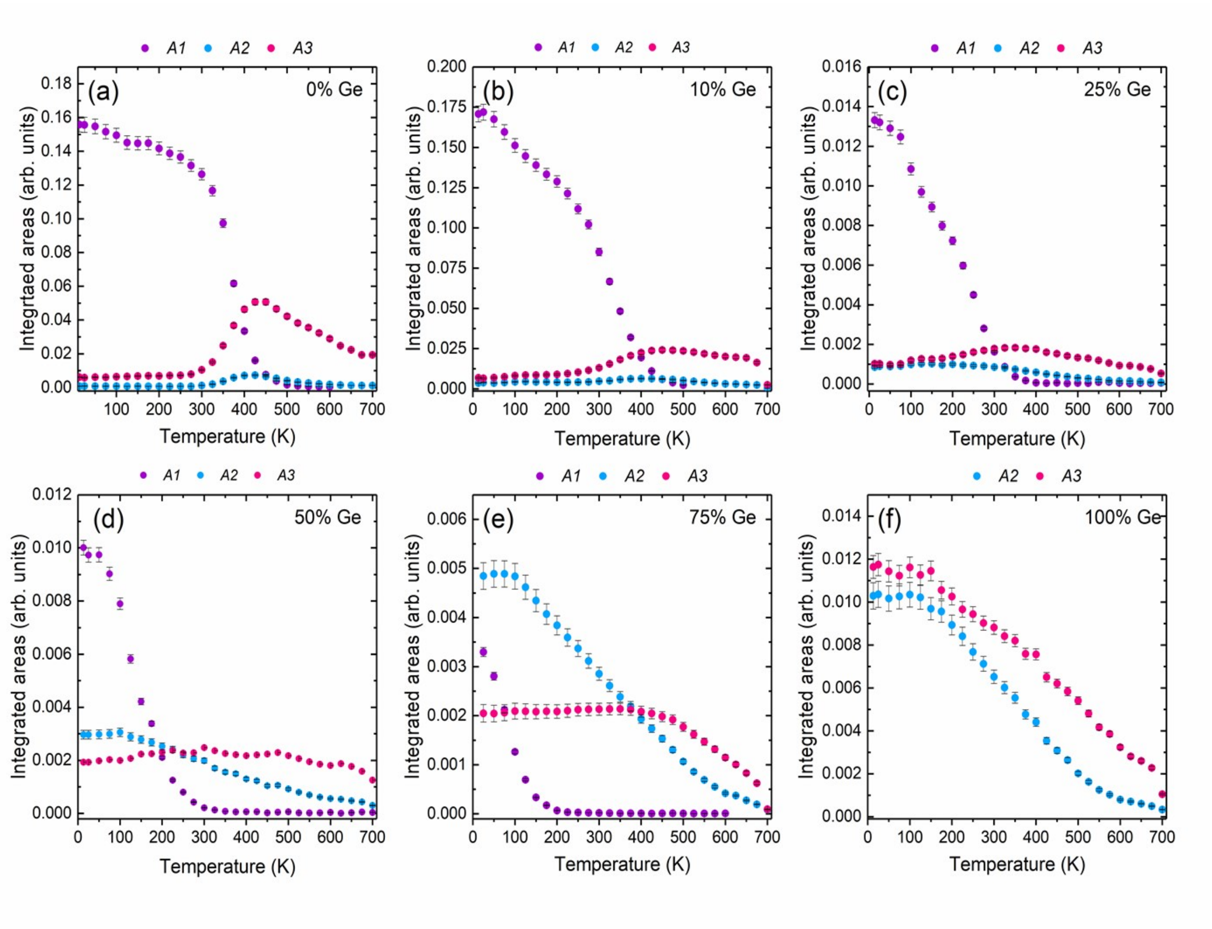

Figure S10. Thermal evolution of the integrated areas (A1, A2, A3 – see Figure S9) of $Y_2(Ge_xSi_{1-x})O_5$:Pr where (a) x = 0, (b) x = 10%, (c) x = 25%, (d) x = 50%, (e) x = 75%, (f) x = 100%.

The uncertainty in determined *LIR* value were calculated according to Eq. S4[12]:

$$\delta LIR = \sqrt{\left(\frac{\delta I_1}{I_1}\right)^2 + \left(\frac{\delta I_2}{I_2}\right)^2} * LIR, \qquad (S4)$$

where $\delta I_i/I_i$ (i=1,2) is estimated through the *SNR* values.

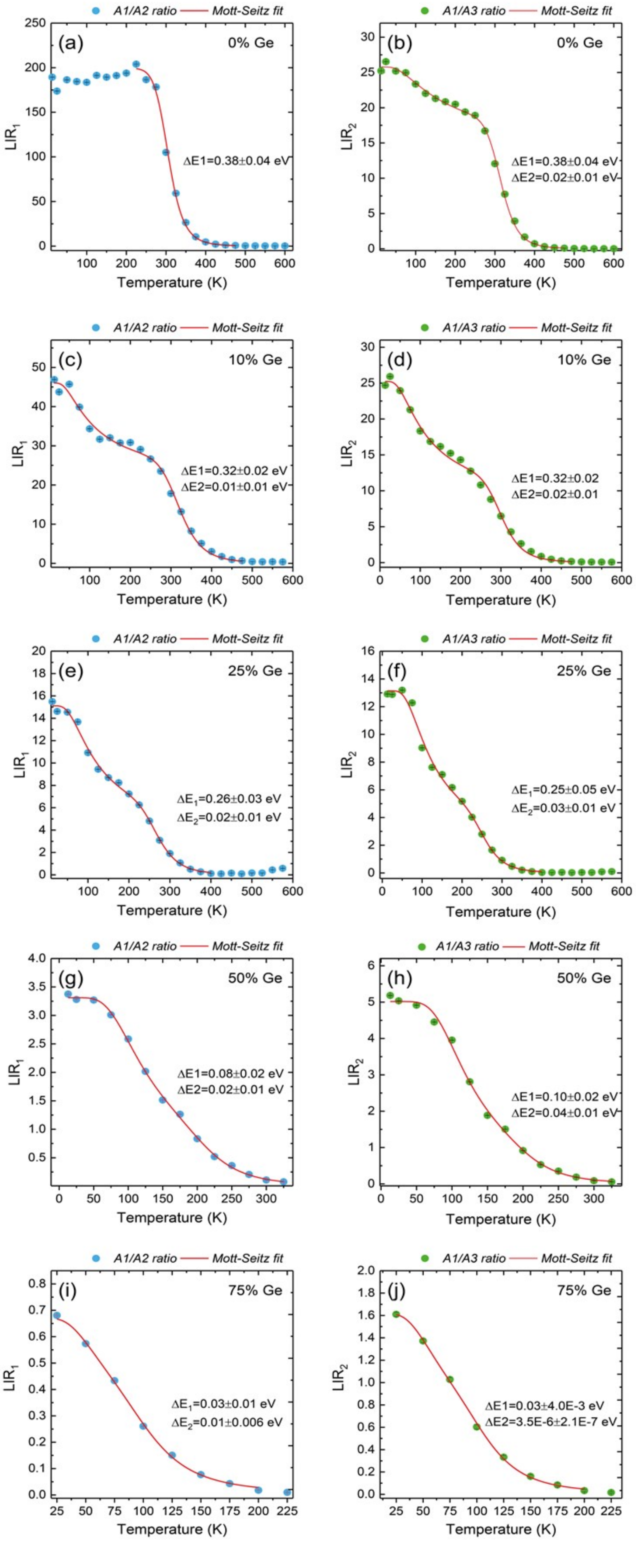

Figure S11. Thermal evolution of LIR_1 and LIR_2 for all the phosphors. The corresponding fitting parameters are presented in Table S5.

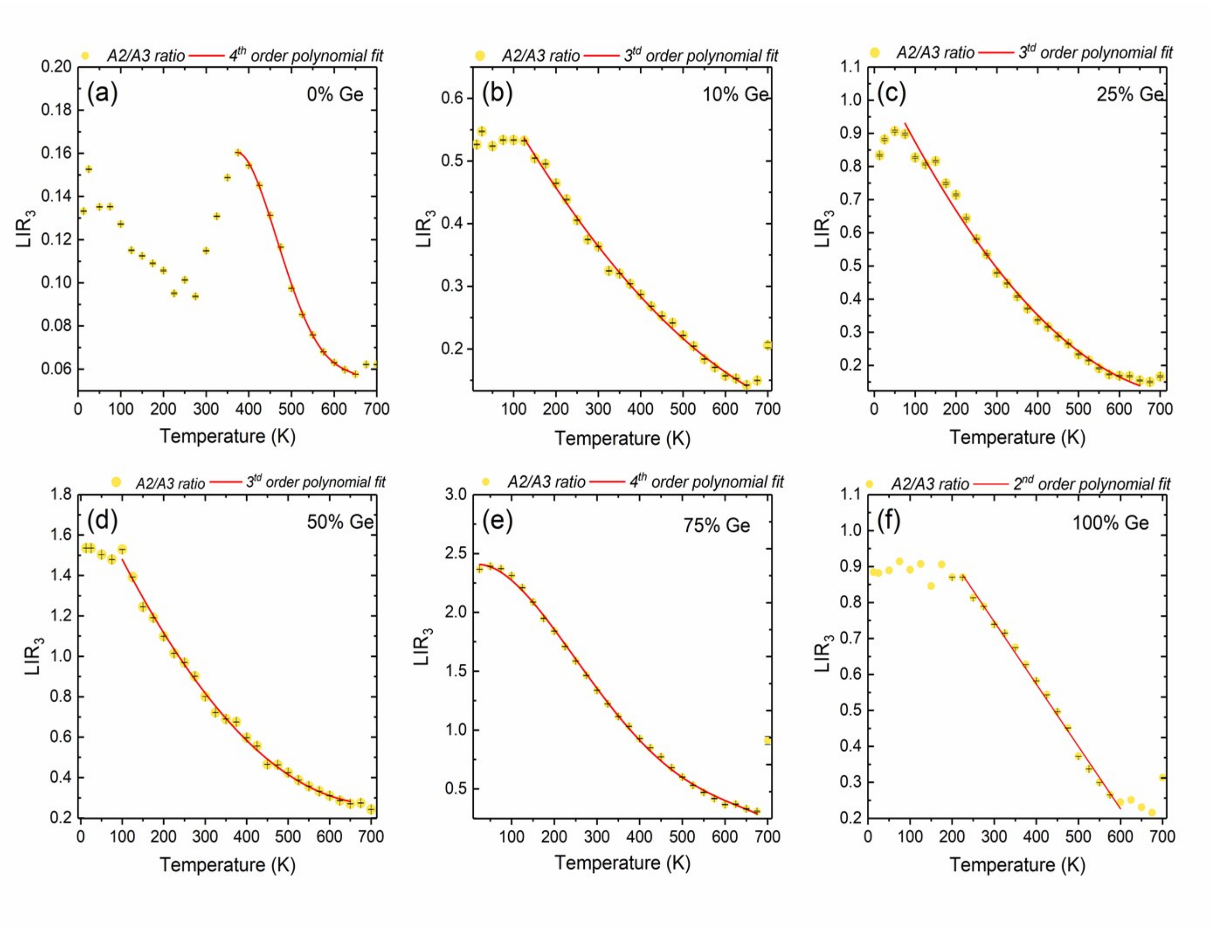

Figure S12. Calibration curves of the $Y_2(Ge_x,Si_{1-x})O_5$:Pr luminescence thermometers using the LIR_3 (A2/A3), where (a) x = 0%, (b) x = 10%, (c) x = 25%, (d) x = 50%, (e) x = 75%, (f) x = 100%.

Repeatability of thermometric parameters

In order to check the stability of the temperature measurement, we performed repeatability tests. The emission spectra were measured in ten consecutive heating-cooling cycles. The repeatability was calculated using of Eq S5:

$$R = 1 - \frac{max(LIR_c - LIR_i)}{LIR_c}, \qquad (S5)$$

where LIR_c stands for the mean thermometric parameter (extracted from the calibration curve), and LIR_i represents the value of thermometric parameter calculated for each cycle. The computed repeatability never drops below 99.4% during the ten cycles, which is a very good result.

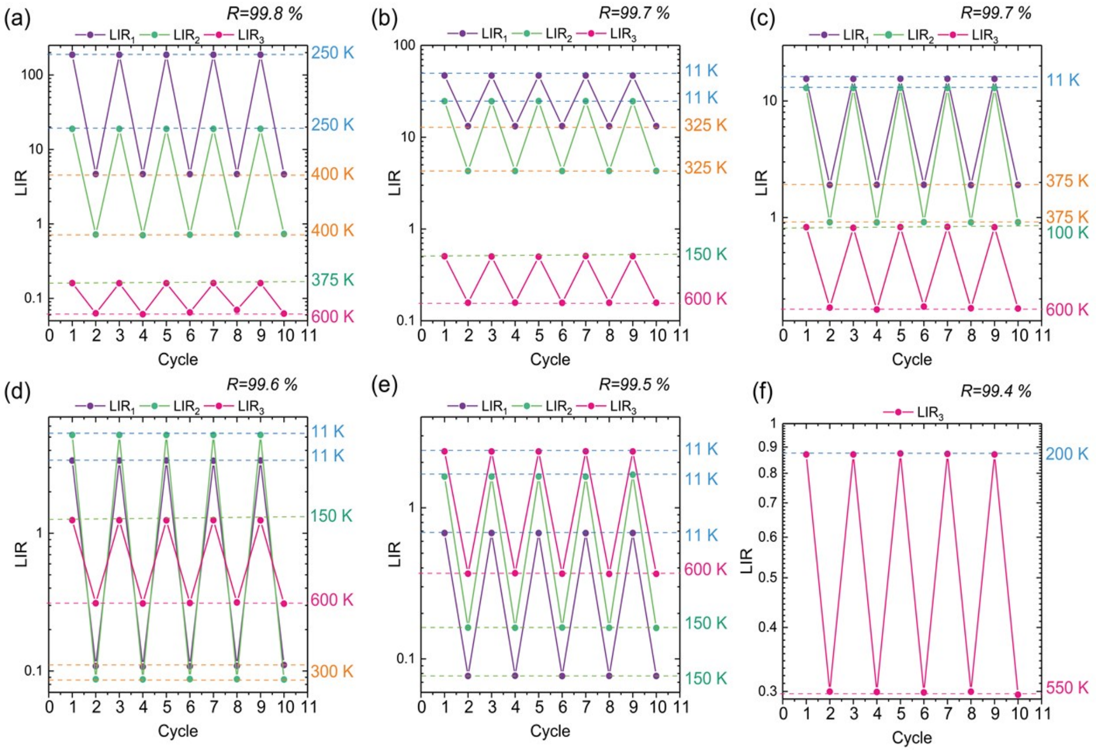

Figure S13. Results of repeatability measurements of $Y_2(Ge_x,Si_{1-x})O_5$:Pr obtained from ten consecutive heating-cooling cycles. For (a) - (e) the presented R values are the lowest (the "worst") of the three calculated for each phosphor.

Relative thermal sensitivity

The calculated relative thermal sensitivities are presented in Figure 6a-c. The error of the obtained S_r is determined by Eq. S6:

$$sS_r = \sqrt{2}\frac{\sigma LIR}{LIR}S_r \qquad (S6)$$

Temperature uncertainty

The temperature uncertainty based on *LIR* (see Eq. 2) was calculated using Eq. S7

$$\delta T = \frac{1}{S_r}\frac{\delta LIR}{LIR}, \qquad (S7)$$

where *δLIR/LIR* was calculated according to Eq. S4. The derived experimental data were fitted with 3rd-order polynomial functions.

The error in δT can be estimated using Eq. S8:

$$s\delta T = \sqrt{2}\frac{\sigma LIR}{LIR}\delta T \qquad (S8)$$

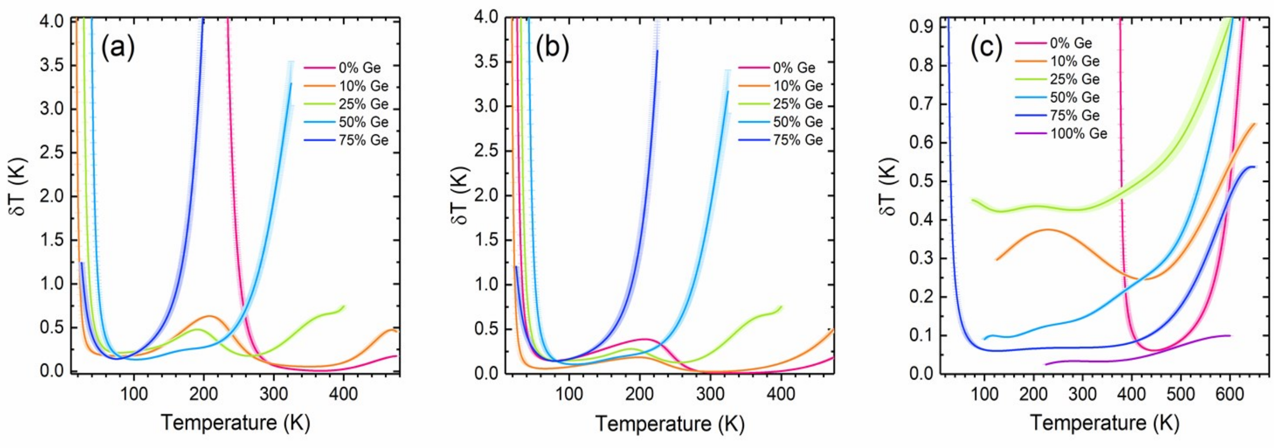

Figure S14. Temperature uncertainty of the $Y_2(Ge_xSi_{1-x})O_5$:Pr luminescence thermometers based on (a) LIR_1, (b) LIR_2, (c) LIR_3.

In the case of temperature uncertainty when the decay times of the 5d→4f luminescence is used Eq. S9 applies:

$$\frac{\delta LIR}{LIR} = \sqrt{2}\frac{\delta\tau}{\tau}, \qquad (S9)$$

from which Eq. S10 could be derived:

$$\delta T = \frac{\sqrt{2}\delta\tau}{S_r\ \tau}, \qquad (S10)$$

whereas δτ stands for the error in determination of τ using the Lavenberg-Marenberg algorithm.

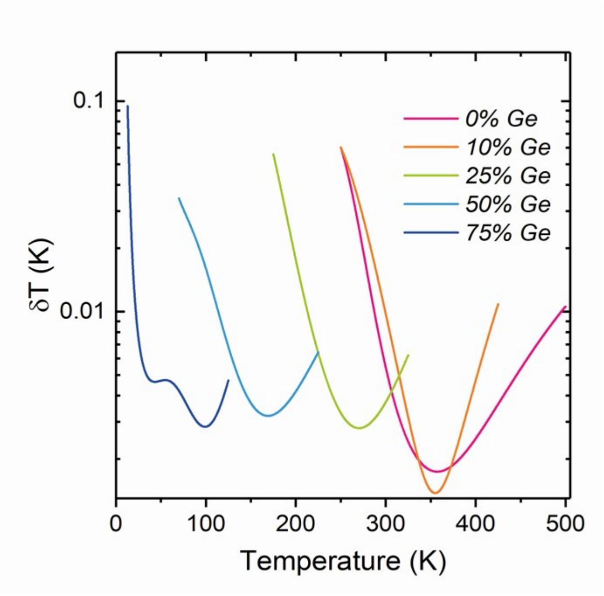

Figure S15. Temperature uncertainty based on 5d→4f emission decay time of the $Y_2Ge_xSi_{1-x}O_5$:Pr phosphors.

Table S1. Experimental data on exciton energy (Eex), charge transfer (ECT), Coulomb repulsion energy (U (6,A)) for $Y_2(Ge,Si)O_5$ host lattices.

x	**E^{ex} (eV)**	**E^{CT} (eV)**	**U (6,A) (eV)**
0	6.80	4.81	6.83
0.10	6.74	4.83	6.83
0.25	6.65	4.85	6.83
0.50	6.50	4.89	6.82
0.75	6.35	4.93	6.82
1	6.20	4.96	6.82

Table S2. 300 K crystal data of Y_2SiO_5 and Y_2GeO_5 derived from Rietveld refinements. See ref [8,9] for more information.

Refined formula	Y_2SiO_5[8]	Y_2GeO_5[9]
Crystal system	monoclinic	monoclinic
Space group; Z	*I*2/a; 8	*I*2/a; 8
Unit cell	a= 10.4207 (3) Å b= 6.7281(2) Å c= 12.4966(3) Å α= 90 ° β= 102.691(2) ° γ= 90 °	a= 10.4706 (2) Å b= 6.8292 (1) Å c= 12.8795 (2) Å α= 90 ° β= 101.750 (3) ° γ= 90 °
Volume	854.751(3) Å^3	901.66 (3) Å^3

Table S3. Calculated decay times of emissions from the $^3P_0$ and $^1D_2$ levels of Pr^{3+} in the $Y_2(Ge_x,Si_{1-x})O_5$ compositions under 250.50 nm excitation. All decay traces were registered at RT.

Composition	**$^3P_0$ level (μs)**	**$^1D_2$ level (μs)**
0% Ge	2.5	122.3
10% Ge	3.2	110.7
25% Ge	4.1	112.3
50% Ge	5.8	127.1
75% Ge	7.0	122.7

100% Ge	8.6	101.6

Table S4. Integration limits used to calculate the integrated areas of the analyzed three transitions.

x Ge	**I_1 (eV)**	**I_2 (eV)**	**I_3 (eV)**
0.00	4.844-3.283	2.654-2.382	2.180-2.009
0.10	4.828-3.376	2.664-2.380	2.200-2.005
0.25	4.813-3.407	2.627-2.373	2.160-2.011
0.50	4.789-3.301	2.627-2.380	2.154-2.016
0.75	4.778-3.300	2.635-2.381	2.131-2.019
1.00	-	2.620-2.383	2.131-2.015

Table S5. Fitting parameters obtained by the Mott-Seitz model for all the $Y_2(Ge_x,Si_{1-x})O_5$:Pr compositions.

The Mott-Seitz model fitting parameters (Eq. 3) for the *LIR*$_1$						
x	**LIR_0**	**α_1**	**ΔE_1**	**α_2**	**ΔE_2**	**r^2**
0.00	192.43±8.83	$(11\pm4) \pm 10^6$	0.38±0.04			0.997
0.10	45.05±2.09	1.20±0.13	0.01±0.006	$(2.34\pm0.3) \pm 10^5$	0.32±0.02	0.991
0.25	15.28±0.72	1.75±0.23	0.01±0.004	$(7.24\pm0.3) \pm 10^3$	0.26±0.01	0.999
0.50	3.25±0.21	13.08±1.21	0.02±0.006	$(8.84\pm0.1) \pm 10^2$	0.08±0.01	0.999
0.75	0.66±0.05	5.50±0.03	0.01±0.006	755.50±18.62	0.03±0.01	0.999
The Mott-Seitz model fitting parameters (Eq. 3) for the *LIR*$_2$						
0.00	25.03±1	0.84±0.23	0.02±0.006	$(9.4\pm0.2) \pm 10^6$	0.38±0.04	0.992
0.10	25.22±0.38	2.16±0.22	0.02±0.001	$(5.78\pm0.3) \pm 10^5$	0.32±0.02	0.997
0.25	15.23±0.08	2.32±0.05	0.02±0.007	$(8.5\pm0.7) \pm 10^3$	0.25±0.01	0.999
0.50	5.08±0.02	1.92±0.11	0.04±0.002	$(2.8\pm0.1) \pm 10^3$	0.10±0.01	0.994
0.75	0.11±0.001	0.72±0.01	0.004±0.001	8.29±0.62	0.03±0.001	0.992

Table S6. Fitting parameters for the *LIR*$_3$(T) dependence of $Y_2(Ge_x,Si_{1-x})O_5$:Pr derived using the polynomial functions.

x	**A_0**	**$A_1 \times 10^{-4}$**	**$A_2 \times 10^{-5}$**	**$A_3 \times 10^{-8}$**	**$A_4 \times 10^{-11}$**	**r^2**
0.00	-3.83±0.37	$(0.32\pm0.1) \times 10^5$	-9.25±0.89	11.4±0.11	-5.19±0.56	0.999
0.10	0.50±0.06	9.46±0.85	-1.19±0.5	3.35±0.58		0.994
0.25	1.11±0.02	$(2.5\pm0.001) \times 10^3$	$(1.61\pm0.004) \times 10^3$	-	-	0.997
0.50	1.87±0.01	$(4.4\pm0.005) \times 10^3$	0.32±0.005	-	-	0.999

0.75	2.37±0.14	-11.79±0.67	-2.86±0.39	-5.21±0.72	-2.91±0.22	0.999
1.00	1.26±0.01	(1.17±0.02) x 10^6	-	-	-	0.995

5. **Literature**

1 P. Dorenbos, *J. Lumin.*, 2000, **91**, 155–176.

2 P. Dorenbos, *J. Phys. Condens. Matter*, 2003, **15**, 8417–8434.

3 P. Dorenbos, *J. Lumin.*, 2003, **104**, 239–260.

4 N. I. Leonyuk, E. L. Belokoneva, G. Bocelli, L. Righi, E. V. Shvanskii, R. V. Henrykhson, N. V. Kulman and D. E. Kozhbakhteeva, *Cryst. Res. Technol.*, 1999, **34**, 1175–1182.

5 R. D. Shannon, *Acta Crystallogr. Sect. A*, 1976, **32**, 751–767.

6 M. S. Buryi, V. V. Laguta, D. V. Savchenko and M. Nikl, *Adv. Sci. Eng. Med.*, 2013, **5**, 573–576.

7 V. Babin, V. V. Laguta, M. Nikl, J. Pejchal, A. Yoshikawa and S. Zazubovich, *Opt. Mater. (Amst).*, 2020, **103**, 109832.

8 K. A. Denault, J. Brgoch, S. D. Kloß, M. W. Gaultois, J. Siewenie, K. Page and R. Seshadri, *ACS Appl. Mater. Interfaces*, 2015, **7**, 7264–7272.

9 E. M. Rivera-Muñoz and L. Bucio, *Acta Crystallogr. Sect. E Struct. Reports Online*, 2009, **65**, i60–i60.

10 J. Mooney and P. Kambhampati, *J. Phys. Chem. Lett.*, 2013, **4**, 3316–3318.

11 G. Blasse and B. . Grabbmaier, *Luminescent Materials*, Springer-Verlag Berlin Heidelberg, 1994.

12 C. D. S. Brites, A. Millán and L. D. Carlos, in *Handbook on the Physics and Chemistry of Rare Earths*, 2016, vol. 49, pp. 339–427.